



1 **3D-Var versus Optimal Interpolation for Aerosol Assimilation: a Case Study**
2 **over the Contiguous United States**

3 Youhua Tang^{1,2} (youhua.tang@noaa.gov), Mariusz Pagowski^{4,5}, Tianfeng Chai^{1,2}, Li Pan^{1,2}, Pius
4 Lee¹, Barry Baker^{1,2}, Rajesh Kumar⁶, Luca Delle Monache⁶, Daniel Tong^{1,2,3}, and Hyun-Cheol
5 Kim^{1,2}

- 6 1. NOAA Air Resources Laboratory, College Park, MD.
7 2. Cooperative Institute for Climate and Satellites, University of Maryland at College Park, MD.
8 3. Center for Spatial Information Science and Systems, George Mason University, Fairfax, VA.
9 4. NOAA Earth System Research Laboratory, Boulder, CO.
10 5. Cooperative Institute for Research in Environmental Sciences, University of Colorado, Boulder, CO.
11 6. National Center for Atmospheric Research, Boulder, CO.

12
13 **Abstract**

14 This study applies the Gridpoint Statistical Interpolation (GSI) 3D-Var assimilation tool
15 originally developed by the National Centers for Environmental Prediction (NCEP), to improve
16 surface PM_{2.5} predictions over the contiguous United States (CONUS) by assimilating aerosol
17 optical depth (AOD) and surface PM_{2.5} in version 5.1 of the Community Multi-scale Air Quality
18 (CMAQ) modeling system. GSI results are compared with those obtained using the optimal
19 interpolation (OI) method (Tang et al., 2015) for July, 2011 over CONUS. Both GSI and OI
20 assimilate surface PM_{2.5} observations at 00, 06, 12, and 18UTC, and MODIS AOD at 18 UTC.
21 In the GSI experiments, assimilation of surface PM_{2.5} leads to stronger increments in surface
22 PM_{2.5} compared to the MODIS AOD assimilation. In contrast, we find a stronger impact of
23 MODIS AOD on surface aerosols at 18 UTC compared to the surface PM_{2.5} OI assimilation. The
24 increments resulting from the OI assimilation are spread in 11×11 horizontal grid cells (12km
25 horizontal resolution) while the spatial distribution of GSI increments is controlled by its
26 background error covariances, and the horizontal/vertical length scales. The assimilations of
27 observations using both GSI and OI generally help reduce the prediction biases, and improve
28 correlation between model predictions and observations. GSI produces smoother result and
29 yields overall better correlation coefficient and root mean squared error (RMSE). In this study,
30 OI uses the relatively big model uncertainties, which helps yield better mean biases, but
31 sometimes causes the RMSE increase due to its localized correction. We also examine and
32 discuss the sensitivity of the assimilation experiments results to the AOD forward operators.

33

34 **1. Introduction**

35 The existing U.S. National Air Quality Forecasting Capability (NAQFC) run by the National
36 Oceanic and Atmospheric Administration (NOAA)/National Centers for Environmental



1 Prediction (NCEP) provides daily 48-hour ozone and PM_{2.5} (particle matters with diameter <
2 2.5 μm) forecasts using the Community Multi-scale Air Quality (CMAQ) modeling system with
3 12km horizontal grid resolution. Many contributions toward improving the NAQFC can be
4 found in literatures, including updated emission, meteorology, chemical mechanism and lateral
5 boundary conditions (Pan et al., 2014; Tang et al., 2008; Lee et al., 2016). However, biases still
6 contaminate current predictions.

7 Chemical data assimilation techniques have been developed to improve initial conditions of
8 chemical transport models (CTM) and yield better prediction ((Elbern et al., 1997, 2000, 2007;
9 Elbern and Schmidt, 1999, 2001; Bocquet et al., 2015) by blending the information from a model
10 estimate (refer to as prior or background) and from observations in certain methods. One method
11 is direct blending, e.g. using observed chemical mass concentrations to correct the modeled mass
12 concentrations, which is relatively straightforward, as they are directly comparable. As most
13 monitoring data are located near surface, that method was usually applied to near-surface field.
14 Another method is indirect guessing, e.g. comparing satellite retrieved AOD with modeled AOD
15 to estimate the biases of modeled column mass concentrations and make the corresponding
16 adjustment. Tang et al. (2015) used both surface PM_{2.5} and MODIS AOD to adjust the initial
17 condition of a CTM with the optimal interpolation (OI) method, and successfully reduced the
18 model biases. The OI correction was applied to 7×7 or 11×11 grid cells horizontally, and from
19 the ground to the boundary layer top vertically for surface PM_{2.5} assimilation. Adhikary et al.
20 (2008) and Chai et al. (2017) also used the similar local OI correction to reduce model biases. A
21 more complex method is using the Gridpoint Statistical Interpolation (GSI) (Wu et al., 2002;
22 Purser et al., 2003a, b), a 3D-VAR method, developed by NOAA/NCEP. It has been applied to
23 assimilate the Goddard Chemistry Aerosol Radiation and Transport (GOCART) aerosols in
24 Weather Research and Forecasting model coupled with Chemistry (WRF-CHEM) with its 3D-
25 var method (Pagowski et al., 2014; Liu et al., 2011). In next sections, we describe the method
26 that extends the GSI to assimilate CMAQ aerosols comparing to the OI correction. A comparison
27 for their one-month performances will be discussed.

28

29 **2. Methodology and Settings**

30 The baseline model setting used in this study is similar to Tang et al. (2015), except that the
31 CMAQ model changed from version 5.0.2 to version 5.1 for more refined chemical mechanisms
32 and physical schemes. The meteorology is provided by the WRF-ARW (version 3.4.1) driven by
33 the NCEP FNL (Final Global Analysis) 1° × 1° analysis field and was reinitialized every 24
34 hour. Both the meteorological and air quality models have 12-km horizontal resolution over the
35 contiguous United States, with 42 sigma layers vertically, and the domain tops at 50 hPa. The
36 detailed setting of the CMAQ model can be found in Tang et al. (2015). In order to compare the
37 two assimilation methods, we assimilate same surface PM_{2.5} data (USEPA Air Quality System



1 (AQS) data) 4 times every day (00Z, 06Z, 12Z and 18Z). The 18Z assimilation uses additional
 2 MODIS AOD data from Terra and Aqua satellites.

3

4 **2.1 Settings for Data Assimilations**

5 In this study, we are comparing two assimilation methods: the optimal interpolation and GSI's
 6 3D-Var. The optimal interpolation is carried in the similar way as described in the OI4 case of
 7 Tang et al. (2015) for assimilating surface PM_{2.5} and aerosol optical depth retrieved from
 8 Aqua/Terra MODIS sensors.

$$9 \quad X^a = X^b + BH^T (HBH^T + O)^{-1} (Y - HX^b) \quad (1)$$

10 where X^a and X^b are the analyzed and background (prior modeled) concentrations or aerosol
 11 optical depth (AOD) data, B and O are the background and observation error covariance
 12 matrices, H is the observational operator and H^T is its matrix transpose, and Y is the observation
 13 vector. The relative uncertainty setting is also same as Tang et al. (2015), in which the
 14 background relative uncertainties have horizontal and diurnal variations. The surface PM_{2.5} OI is
 15 applied from surface to the height of the planetary boundary layer (PBL), and the MODIS AOD
 16 is used to adjust above-PBL aerosol after deducting the adjusted below-PBL AOD.

17 The GSI's 3D-var uses a similar approach (Pagowski et al., 2014; Liu et al., 2011) for its cost
 18 function

$$19 \quad J = \frac{1}{2} (x_a - x_b)^T B^{-1} (x_a - x_b) + \frac{1}{2} (Hx_a - O_o)^T O^{-1} (Hx_a - O_o) + Jc \quad (2)$$

20 Where x_a and x_b are the analyzed and background (a prior modeled) concentrations or AOD data,
 21 B and O are the background and observation error covariance matrices, H is the observational
 22 operator, O_o is the observations and J_c is the constraint terms. Both GSI's 3D-Var and OI use
 23 spatially varied background bias and observation to make the adjustment. However, the OI
 24 adjustment is made in each 11×11 grid horizontally and its effect expands up to the PBL height.
 25 The GSI's cost function reduction is performed for the whole domain, and its effect of the
 26 adjustment can be expanded in much greater horizontal and vertical scales defined by its
 27 horizontal and vertical length scales, respectively.

28 In this study, we carry out the similar uncertain setting for the OI as Tang et al. (2015), in which
 29 the background's relative uncertainties have horizontal and diurnal variations (Figure 2 of Tang
 30 et al., 2015) for PM_{2.5} assimilation. For OI's AOD assimilation, we use the fixed relative
 31 uncertainty of 0.8 for modeled AOD. The relatively uncertainties for MODIS AOD and surface
 32 PM_{2.5} observation are same: 0.1. GSI's setting is similar to Pagowski et al. (2014), in which the
 33 background error and length scales have vertical variance. Figure 1 shows that the vertical



1 profiles of background errors and length scales for PM_{2.5} (for PM_{2.5} assimilation) and
2 accumulation-mode sulfate (ASO4J, for AOD assimilation), which can be calculated using GSI's
3 NMC (National Meteorological Center) method (Parrish and Derber, 1992). ASO4J is one of
4 CMAQ aerosol species used in AOD data assimilation. Other aerosol species have proportional
5 model or background errors. The uncertainties of modeled aerosols are high in the lower layers
6 and decrease with altitudes. The model's horizontal length scale indicates the extent of the
7 assimilation's horizontal expansion. In Figure 1, the horizontal length scale for modeled PM_{2.5}
8 increases significantly around the altitude of 12km, where the tropopause is usually located. The
9 model's vertical length scale indicates the extent of the assimilation's vertical expansion, which
10 is related to the strength of vertical advection, diffusion, and convection. Below PBL, the vertical
11 length scale is usually stronger than that in the upper layers. We use the same constant
12 observation error of 0.1 in GSI for surface PM_{2.5} and MODIS AOD. In both settings of GSI and
13 OI, their background errors are far greater than the observation errors in lower altitudes, which
14 push the adjusted values toward the observed surface PM_{2.5}. For AOD assimilations, GSI's main
15 increment is also in low altitudes due to its background error profile (Figure 1), while OI's AOD
16 assimilation applies one adjusting ratio to whole column for each grid cell.

17 2.2 Calculations of Aerosol Optical Depths

18 To assimilate AOD in the CMAQ model, we need convert CMAQ aerosol chemical
19 compositions. CMAQ includes two methods for calculating AOD: the Mie method and the
20 reconstruction method (Binkowski and Roselle, 2003). The Mie method calculates the aerosol
21 optical extinction coefficient (AOE) from modeled aerosol physical characteristics, including the
22 index of refraction, volume concentration and aerosol size distributions. It does not require
23 aerosol chemical composition information and can handle the aerosols' internal mixture, in
24 which each aerosol particle is composed of a solid core and coating layers of various
25 compositions due to the aerosol uptake. In theory, the Mie method should yield accurate AOE if
26 all the model's aerosol physical properties are correct. However, that condition was hard to reach
27 in many circumstances. Also, aerosol mass concentrations are often available in both models and
28 observations, and a convenient method is needed to directly convert aerosol mass concentrations
29 to AOE. So, CMAQ provides another empirical approach, the reconstruction method (RM),
30 which uses the mass concentrations of aerosol chemical compositions to calculate the total AOE
31 with a look-up table. The RM assumes that all aerosols are externally mixed. It calculates each
32 composition's AOE, and sums them up to get the total AOE (Binkowski and Roselle, 2003) for
33 the wavelength of 550nm.

$$34 \quad AOE \left[\frac{1}{km} \right] = 0.003 * f(RH) * \{(NH_4)_2SO_4 + NH_4NO_3\} + 0.004 * \{organic\ mass\} + 0.01 * \\ 35 \quad \{light\ absorbing\ carbon\} + 0.001 * \{fine\ soil\} + 0.0006 * \{coarse\ mass\} + 0.00137 * \\ 36 \quad f_s(RH) * \{sea\ salt\} \quad (3)$$



1 In CMAQ's RM, only the AOE from ammonium, sulfate, nitrate, and sea salt have the
2 dependence on relative humidity (RH). $f(RH)$ and $f_s(RH)$ are two RH-dependent look-up tables
3 of aerosol hygroscopic growth for sulfate/nitrate/ammonium and sea salt, respectively (the
4 original RM (Binkowski and Roselle, 2003) in earlier versions (<5.1) of CMAQ does not include
5 sea salt's RH dependence for AOE calculation). All other aerosols are converted from their mass
6 concentrations to the corresponding AOE with simple fixed constants. The conversion method
7 does not need aerosol size distribution, but just the mass concentrations of aerosol compositions
8 and ambient RH. Due to its simplicity and convenience, the RM method is widely used not only
9 for CMAQ aerosols, but also for converting observed aerosol mass concentrations to AOE
10 (Malm et al., 1994; Roy et al., 2007). Tang et al. (2015) also use the RM calculated AOD for OI
11 assimilation, which is carried out here for this OI assimilation. In contrast, the Mie method based
12 on aerosol physical characteristics is relatively hard to be used in data assimilations, as the data
13 assimilations target the mass concentrations of aerosol compositions, not the aerosol physical
14 characteristics directly. Although we can use adjusted aerosol mass concentrations to calculate
15 the corresponding change on aerosol physical characteristics with CMAQ routines, and then link
16 it to AOD adjustment, the additional conversion makes these calculations difficult.

17 In theory, we should use the same forward method, such as RM, to calculate AOD used in GSI.
18 However, the CMAQ's current RM is relatively simple, only for single wavelength, 500nm,
19 without considering aerosol distribution. The current RM can not be directly used to calculate
20 multi-wavelength AOD, though this study only uses the 550nm AOD. The existing GSI has its
21 own tool, the Community Radiative Transfer Model (CRTM, Han et al., 2006; Liu and Weng,
22 2006), to handle its AOD calculation. CRTM provides GSI not only the forward AOD, but also
23 the calculations of tangent-linear, adjoint and K-matrix for multiple wavelengths. As the GSI is
24 tightly coupled with CRTM for its AOD related operations, we need to go through the CRTM for
25 utilizing GSI's existing AOD assimilation capability. However, the current version of CRTM
26 does not support CMAQ's aerosol species, and only handle GOCART (Goddard Chemistry
27 Aerosol Radiation and Transport, Chin et al., 2000, 2002) aerosol species. GOCART's aerosol
28 species are similar to the classification of aerosol used in CMAQ RM method, including sulfate,
29 dust, sea salt, black carbon, and organic carbon, which also assumes that the aerosols are
30 externally mixed. It is possible for us to represent CMAQ aerosols in GOCART aerosol
31 categories for calculating their optical properties. Table 1 shows how the CMAQ 5.1 Aero6
32 species (Sonntag et al., 2014) are mapped to CRTM's GOCART aerosol. CMAQ aerosols have
33 3 size modes: Aitken (i-mode), accumulation (j-mode) and coarse mode (k-mode) representing
34 the super-fine nucleation particles, aged coagulated particles, and coarse particles, respectively
35 (Binkowski and Roselle, 2003). Each size mode has its own lognormal size distribution (Whitby
36 and McMurry, 1997). We applied the CMAQ averaged aerosol size for each mode (aitken,
37 accumulation or coarse) to the CRTM AOD calculation. Unlike the CMAQ RM method in
38 which only AOE from sulfate, nitrate, ammonium and sea salt have RH dependence, all the
39 calculations for GOCART AOE except hydrophobic BC/OC depend on ambient RH,
40 wavelength and aerosol sizes, which differs from RM's one-size-fit-all method.



1 Figure 2 shows one example of the AOD calculations from the 3 methods mentioned above
 2 compared to Terra/Aqua MODIS AOD data. The MODIS AODs in Figure 2 are the daily data,
 3 and the overpass times of Terra and Aqua satellites on 07/01/2011 ranges from 15 to 22 UTC
 4 over the CONUS. Both OI and GSI use the AOD assimilation window of +/- 2 hours. During this
 5 event, some wildfire occurred in Southern Canada-Wisconsin, North and South Carolinas, which
 6 caused the relatively high AOD values. These high AODs are also confirmed by the MODIS
 7 retrievals (Figure 2d). Figure 2 shows that the different AOD calculations from the same CMAQ
 8 aerosol mass loadings yield the similar spatial distribution pattern with noticeable quantitative
 9 differences, and in general we see RM AOD > Mie AOD > CRTM AOD. In most regions,
 10 especially over Western USA, e.g. Nevada, MODIS AOD is higher than the three CMAQ AODs.
 11 The Mie-method AOD and CRTM AOD are generally lower than MODIS AOD. Only RM
 12 method shows some sporadic overestimated AOD over Southern Canada-Wisconsin and
 13 Carolinas. These differences will lead to the corresponding differences in data assimilation
 14 adjustments. Roy et al. (2007) compared the CMAQ AODs with surface AOD observations from
 15 the nephelometer instrument over 25 Interagency Monitoring of Protected Visual Environment
 16 (IMPROVE) sites (most of them were located in National Parks), and found that the CMAQ RM
 17 method yielded too high surface AOD, but agreed well with AEORNET (Aerosol Robotic
 18 Network) and MODIS AOD in summer 2001. In Roy et al. (2007), CMAQ used static lateral
 19 boundary condition, which may miss some elevated aerosol loadings (Lu et al., 2016). It is very
 20 likely that their CMAQ overpredicted near-surface AOD loading and underpredicted elevated
 21 AOD loading, but got total column AOD in right magnitude. In another word, the converting
 22 factors of RM method used in equation (3) may be too high if their CMAQ predicted correct
 23 aerosol mass concentration over those National Park sites.

24 2.3 PM_{2.5} Calculations

25 Besides the MODIS AOD, The data assimilations of OI and GSI also use surface PM_{2.5}
 26 observations to make adjustments. The OI method for surface PM_{2.5} assimilation was described
 27 in Tang et al. (2015). Pagowski et al. (2014) described the GSI method for surface PM_{2.5}
 28 assimilation used in WRF-CHEM in which aerosol size bins are fixed. CMAQ's PM_{2.5}
 29 calculation is slightly different as it is not defined by fixed size bins, but three size modes:
 30 Aitken, accumulations and coarse modes (i, j, k modes) (Appel et al., 2010).

$$\begin{aligned}
 31 \quad PM_{2.5} = & PM_{25AT} * (SO4_i + NO3_i + NH4_i + Na_i + Cl_i + EC_i + POC_i + OTHER_i) + \\
 32 \quad & PM_{25AC} * (SO4_j + NO3_j + NH4_j + Na_j + Cl_j + EC_j + EL_j + POC_j + SOA_j + OTHER_j) + \\
 33 \quad & PM_{25CO} * (SO4_k + NO3_k + NH4_k + Na_k + Cl_k + SOIL_k + OTHER_k) \quad (4)
 \end{aligned}$$

34 where PM_{25AT}, PM_{25AC} and PM_{25CO} are the mass scaling factors for the three modes,
 35 indicating the mass ratios of each mode falling in PM_{2.5} size range (Jiang et al., 2006), and their
 36 value ranges should be between 0 and 1. POC is the primary organic carbon, and SOA represents
 37 the 23 secondary organic aerosols (table 1). CMAQ 5.1 also includes 8 additional mineral
 38 elements: Fe, Al, Si, Ti, Ca, Mg, K and Mg (Table 1) in its accumulation mode, represented by



1 *EL_j*. The species *OTHER* represent all other aerosols (Table 1) in each mode. The equation 4
2 describes the forward operator for calculating $PM_{2.5}$, which is feed into GSI as background $PM_{2.5}$
3 concentration. After the GSI estimates the total $PM_{2.5}$ increment, the increment is proportionally
4 allocated to each aerosol size mode with the corresponding mass scaling factor, and then to each
5 aerosol species. Thus, the final adjustment that OI and GSI give back to CMAQ is the mass
6 concentration increment for each aerosol species, and it does not change their size distributions,
7 which is also the effect of AOD assimilation.

8 **3. Results and Discussions**

9 As the GSI and OI methods assimilate both surface $PM_{2.5}$ and AOD, the impacts of these
10 adjustments can be compared. Figure 3 shows the CMAQ raw predictions (referred to as base-
11 case run) of surface $PM_{2.5}$ compared to the measurements. In most regions west of $100^{\circ}W$, this a
12 priori case underestimated the surface $PM_{2.5}$. Surface measurement also shows some sporadic
13 high $PM_{2.5}$ values in Eastern USA, missed by the base-case run. The goal of the data
14 assimilations is to reduce these errors.

15 **3.1 The Impact of Data Assimilation on Aerosol Mass Concentration**

16 Since both $PM_{2.5}$ and aerosol AOD represent the concentrations of 54 aerosol species (Table 1),
17 to understand the data assimilation method performances, we choose the accumulation-mode or
18 J-mode sulfate (ASO4J), to illustrate the impact of data assimilation. Other aerosol species have
19 proportional adjustments in the GSI and OI assimilations. Figure 4 (a, b) shows that the GSI
20 assimilation with surface $PM_{2.5}$ yields more significant changes than the corresponding OI
21 assimilation. The OI assimilation of $PM_{2.5}$ leads to more localized increments compared to GSI
22 since OI increment is spread over 11×11 grid cells (i.e., an area of 17424 km^2), while GSI
23 increment spread depends on the horizontal length scales. Their adjustments also differ over
24 certain areas. For instance, the base case underestimates $PM_{2.5}$ in Chicago, but it overestimates
25 $PM_{2.5}$ in southeastern Wisconsin (Figure 3). The OI adjustment has a local flavor: increase
26 ASO4J in Chicago, and decrease it over southeastern Wisconsin (Figure 4b). The GSI's result
27 differs significantly due to its length scales and cost-function reduction over the whole domain. It
28 yields overall $PM_{2.5}$ reduction in Chicago surrounding areas with smaller correction. Similar
29 differences are also noted in other areas and other periods.

30 The impacts of AOD assimilations via GSI and OI also differ significantly (Figure 4c, 4d). The
31 model relative uncertainty used in the OI assimilation is relatively high, which caused the strong
32 adjustment in ASO4J (Figure 4d) due to OI's AOD assimilation over Nevada-Southern
33 California, Illinois and Michigan. The OI assimilation of AOD increases ASO4J over most of the
34 model domain except in certain areas, such as Northeastern Minnesota-Southern Canada, and the
35 eastern part of the border of North Carolina and South Carolina where the OI assimilation leads
36 to a decrease in ASO4J (Figure 4d). The GSI assimilation of AOD tends to be more moderate
37 and smoother. Its increment is almost one order of magnitude smaller than the variation of OI-



1 AOD assimilation (Figure 4c). Figure 4c shows that the majority of increments of GSI-AOD
2 assimilation occur in Eastern California-Nevada, Missouri-Illinois (St. Louis surrounding areas)
3 and Wisconsin.

4 Figures 4e and 4f show the combined effect of assimilation of both surface $PM_{2.5}$ and AOD on
5 surface $ASO4J$ from GSI and OI methods, respectively. For GSI, the impact of assimilating
6 surface $PM_{2.5}$ is greater than that of assimilating MODIS AOD. The OI assimilations show the
7 opposite effect with AOD assimilation having a bigger impact than its surface $PM_{2.5}$
8 assimilation.

9 It should be noted that the difference between GSI and OI increments is not only on their
10 horizontal distribution, but also on their vertical distribution. GSI has a height-dependent
11 background error profile (Figure 1) while OI applies the uniform adjustment ratio to either whole
12 column for AOD assimilation or below PBL for surface $PM_{2.5}$ assimilation. Figure 5 shows the
13 model predicted PBL height at this time. In most portions of CONUS domain except the Rocky
14 mountain region, the PBL height is less than 3 km. It means that the impact of OI- $PM_{2.5}$
15 assimilation should be below 3 km for most regions. Considering the locations of available
16 surface $PM_{2.5}$ monitoring stations and the regional distribution of background $PM_{2.5}$, the vertical
17 extension of the increments of OI- $PM_{2.5}$ should be more limited. Figure 6 shows the $ASO4J$
18 increments similar to Figure 4 but for the model's 18th layer, or roughly 2 km above ground.
19 Figure 6b shows that the OI- $PM_{2.5}$ adjustment at the 2 km layer only appears in sporadic
20 locations, such as Raleigh/Durham (central North Carolina), Atlanta and Denver downwind
21 areas. Compared to Figure 4b and 5, we can find that in the most CONUS regions, the OI-
22 $PM_{2.5}$'s $ASO4J$ increments do not show up in the 2km layer because either their PBLs are lower
23 than 2km, or there is no strong surface adjustment due to the locations of monitoring stations. On
24 the contrary, GSI- $PM_{2.5}$ assimilation shows the horizontal distribution of $ASO4J$ increment at
25 2km similar to its surface increment (Figure 6a, 4a), but with a much smaller magnitude than the
26 increment of OI- $PM_{2.5}$ assimilation at the 2 km layer. The GSI-AOD assimilation also yields a
27 similar $ASO4J$ adjustment pattern with smaller increments than OI-AOD (Figure 6c, 4c). The
28 strongest adjustment at the 2 km layer comes from the OI-AOD assimilation, which uses the
29 same adjustment ratio for the whole vertical column. Its impact on 2 km $ASO4J$ is more than one
30 order of magnitude stronger than the corresponding GSI assimilation due to its relatively high
31 uncertainty setting. In term of combined effect at the 2km, for GSI, the AOD assimilation is
32 almost equally important as the surface $PM_{2.5}$ assimilation, depending on regions (Figure 6e).
33 For OI assimilation, the AOD's impact is dominated at the 2km layer as the surface $PM_{2.5}$'s
34 effect only appear sporadically (Figure 6f).

35 **3.2 The Impact of Data Assimilation on AODs**

36 The above discussion is about the data assimilations' impacts on one aerosol mass concentration.
37 It is also still needed to assess the impacts on column AODs, as the AOD is used here to make
38 assimilations. Fortunately both CRTM and RM are composition-based methods for externally



1 mixed aerosols, and we can easily calculate the AOD changes due to the changes of aerosol mass
2 concentrations. Figure 7 shows the CRTM AOD changes due to GSI assimilation (left panel),
3 and RM AOD changes due to OI assimilation (right panel). Their spatial distribution patterns are
4 very similar to the corresponding surface ASO4J increments in Figure 4 as most high aerosol
5 loadings are near surface. However, the AOD increment's value range of GSI-PM_{2.5} assimilation
6 is more than one order of magnitude lower than that of OI-PM_{2.5}. One reason is that the CRTM
7 method yields 2 or 3 times lower AOD than the RM method with same aerosol loading (Figure
8 2b, 2c). Another reason, or the major reason, is that GSI-PM_{2.5} assimilation has much lower
9 increment on total aerosol mass loading, reflected by the magnitude difference between Figure
10 6a and 6b, as the GSI assimilation uses a steepen background error profile (Figure 1), makes its
11 major adjustment near surface and yields smaller overall adjustment for total column aerosol
12 mass loading. On the contrary, the OI-PM_{2.5} assimilation applies the same adjustment ratio to the
13 aerosol masses below PBL, and the adjustment could be much stronger than that of GSI-PM_{2.5}
14 assimilation for the elevated layers blow PBL. We can see the similar patterns and differences
15 due to their AOD assimilations (Figure 7c, 7d). The AOD increments due to GSI-AOD and OI-
16 AOD have the similar horizontal distribution to their corresponding ASO4J mass increments
17 (Figure 4c, 6c and 7c; Figure 4d, 6d, and 7d), but the OI-AOD has much stronger adjustments on
18 total AOD and elevated aerosol masses. Generally, the GSI-AOD tends to increase AOD or
19 aerosol column loading in Northern Central USA and over Nevada (Figure 7c). The OI-AOD
20 assimilation has the similar AOD increment over these two regions, but decrease AOD or aerosol
21 column loading over Texas, Northern Florida, South Central Canada, and the border of North
22 Carolina and South Carolina (Figure 7d). It should be noted that the OI-PM_{2.5} assimilation yields
23 the AOD enhancements in Southern and Eastern USA, though just sporadically (Figure 7b). So
24 there is a conflict as the OI-PM_{2.5} and OI-AOD assimilations pointed to opposite adjusting
25 directions over some areas, implying that the RM AOD could yield some overpredictions. Under
26 this situation, the combined OI assimilations will increase below-PBL aerosol masses according
27 to the adjustment of OI-PM_{2.5}, but reduce the above-PBL aerosol mass to fit the overall AOD
28 reduction and get compromised results over these two regions (Figure 7f). This conflict-
29 resolving process will change the vertical distribution of CMAQ aerosols. Figure 7 shows that
30 the overall AOD increments are mainly due to PM_{2.5} assimilation in GSI, and AOD assimilation
31 in OI. The OI adjustments on AOD are much stronger than that of GSI, which is mainly due to
32 their adjustments at the elevated layers.

33 **3.3 The Overall Assimilation Impacts over Longer Periods**

34 We continue the CMAQ runs after the 18UTC assimilations. After 1 hour, or at 19UTC, we
35 compared their surface PM_{2.5} prediction with the corresponding measurement again to see their
36 impacts (Figure 8). At this time, the effects of data assimilations have been transported to
37 downstream areas. Without the data assimilation, the base case (Figure 8a) systematically
38 underestimated the PM_{2.5} in western USA, which is consistent with that shown in Figure 3. Both
39 assimilations correct some of the biases, which is more obvious in areas west of 90°W. For



1 instance, both assimilations correct the $PM_{2.5}$ underprediction in Iowa. In some locations, OI gets
2 better result, such as in Southern Nevada-Southern Utah, and Kansas where only one surface
3 observation is available. In other locations, the GSI achieves better results, such as Southeastern
4 Wisconsin. Sometimes the data assimilations could overcorrect and yield worse results than the
5 base run, such as the OI's overestimation over the Lake Michigan and GSI's overprediction over
6 central Illinois (Figure 8b, 8c). The overcorrection issue is more evident in the OI run as the
7 adjustment of the OI assimilation is stronger than that of GSI, due to OI's stronger setting for
8 model uncertainties. This strong setting is actually helpful sometimes, for instance, the OI
9 assimilation is strong enough to correct the underpredicting bias over southeastern North
10 Carolina, where GSI's moderate correction only helps reduce that bias. The most evident side
11 effect of the OI's overcorrection is the increase of root mean squared error (RMSE).

12 In this study, we employ 4-cycle per day data assimilations, the MODIS AOD assimilation is
13 only applied at the cycle of 18 UTC for both the GSI and OI. We continue these runs for the
14 whole July 2011. Figure 9 shows the time-series plots of these CMAQ predictions for surface
15 $PM_{2.5}$, their correlation coefficient (R) and RMSE. Before July 14 or Julian day 195, the CMAQ
16 base prediction systemically underpredicted the $PM_{2.5}$. After that date, the base model tends to
17 underpredict during daytime, but slightly overpredict during nighttime, except for the last 3 days
18 of July 2011 while the overall underprediction appeared again. Both GSI and OI help reduce these
19 underprediction biases. The OI's correction is stronger due to its stronger setting. It became more
20 evident during the $PM_{2.5}$ peak period caused by the firework emission at night of July 4th (U.S.
21 Independence Day), which is about early morning of July 5th (Julian day 186) in UTC time
22 (Figure 9a). The OI assimilation caught the firework caused $PM_{2.5}$ spike though its peak time
23 was later than that of the observation. The GSI assimilation showed the moderate correction
24 which was not strong enough to full match with observation. The OI run shows some
25 overprediction during the nighttime, especially in later July. Figure 9b clearly shows the effect of
26 4 assimilations per day, represented by the 4-time-per-day enhancement of GSI and OI's
27 correlation coefficients. For the most of this month, we can generally see $GSI > OI > CMAQ$ base
28 for R. The difference of R between GSI and OI is much smaller than that between the
29 assimilations runs and the CMAQ base case. GSI's R is consistent better than the CMAQ base
30 while the OI's R is not always better, e.g. during the Julian days of 191 and 207, though we can
31 still find several periods when OI yielded the highest R. In term of RMSE, the GSI's RMSE is
32 always lower than that of the base run, and the OI run shows some RMSE spikes (Figure 9c) due
33 to its localized correction and strong settings.

34 Table 2 shows the corresponding statistics for the whole domain and the certain regions. The
35 CMAQ base case systematically underpredicted surface $PM_{2.5}$ with mean bias of $-2.25 \mu g/m^3$
36 over CONUS during this period. With data assimilations, the OI and GSI runs get mean biases of
37 0.77 and $-0.73 \mu g/m^3$, respectively. Besides that effect, their correlation coefficient, R, is also
38 improved: the base case's R is 0.3, and Rs of OI and GSI runs are 0.38 and 0.44 over CONUS,
39 respectively. Their indexes of Agreement (IOA) have the corresponding improvements, too.



1 Among the regions, the data assimilation yield most significantly improvements over the Pacific
2 Coast and Southeastern USA, where the CMAQ base case has relatively poor correlation
3 coefficients. In all of these regions, the GSI yields overall best correlation coefficient and RMSE,
4 while the OI run has the smallest mean biases except for South Central region where the GSI's
5 mean bias is the lowest. OI's localized correction and strong settings help get better mean biases,
6 but cause the overcorrection issue and increase RMSE. Over Northeastern USA where relatively
7 dense surface observations are available, the OI's RMSE increase is relatively small. Although
8 both assimilations generally improve the PM_{2.5} prediction, their performance can be highly
9 varied depending on regions. For instance, over Rocky Mountain States where both surface
10 observation and MODIS AOD are limitedly available with complex terrains, the GSI and OI
11 assimilations slightly improve the R and IOA, though they evidently improve the mean bias of
12 surface PM_{2.5}.

13 All these runs have daytime underprediction bias issue from 12 to 00UTC. The 4-cycle-per-day
14 data assimilations help reduce that bias, but the bias trend is still there. It implies that the data
15 assimilation for CMAQ's initial condition has certain limitation, and may not be able to solve the
16 prediction bias by it alone. In addition to uncertainties in initial conditions, forecasts errors also
17 depend on errors in model's meteorology, chemistry and emissions, and we need other
18 adjustments to correct these biases.

19

20 4. Conclusions

21 In this study, we expanded the GSI assimilation to CMAQ 5.1's Aero6 aerosol species. The 4-
22 cycle-per-day aerosol data assimilation for surface PM_{2.5} and AOD were carried out with GSI
23 and OI (Tang et al., 2015) methods over the CONUS. The results were compared against surface
24 PM_{2.5} observation, and shows that both assimilations generally improved the aerosol predictions.
25 The increments resulting from the OI assimilation are spread in 11×11 horizontal grid cells while
26 the increment spread in GSI (a 3D-Var assimilation technique) is controlled by its background
27 error variances, horizontal and vertical length scales. GSI's cost function reduction is performed
28 for the whole domain. The differences in formulation of GSI and OI led to their different patterns
29 of adjusting the initial conditions, and GSI yielded smoother and horizontally broader
30 adjustment, but much weaker vertical increment. OI uses a simple one-ratio-fit-all method for its
31 vertical adjustment up to PBL height for PM_{2.5} assimilation, or whole column for AOD
32 assimilation. OI can use strong setting to achieve better mean bias, but has side effect of RMSE
33 increase due to its localized correction. Overall, GSI's adjustment yield better results even with
34 its moderate setting of data assimilation parameters, showed by its better statistics. One
35 important reason is that GSI's whole-domain cost function reduction, which helps constrain its
36 RMSE, and longer horizontal length scale, especially for PM_{2.5} assimilation (Figure 1), which
37 helps expand its adjusting effect to relatively broad areas. Both assimilations highly depend on



1 the available observations. Compared to GSI's massive code, the OI code is much smaller and
2 portable, which may be good choice of some light-duty usages.

3 AOD assimilations have more issues than the surface $PM_{2.5}$ assimilation, which is not only about
4 the methods for converting aerosol mass concentrations to AOD that relies on the model for
5 ambient RH, aerosol sizes and speciation, but also depends on a prior model for the aerosol
6 vertical distribution. The CRTM AOD is about 2-3 times lower than RM AOD with the same
7 aerosol mass loadings (Figure 2). From the existing evidence, the converting factors used in RM
8 AOD may be too high (Roy et al., 2007), or the RM's one-size-fit-all method may not resolve
9 highly-varied aerosol size impact on AOD calculation. There is another issue of aerosol
10 specification, which is particular important for organic aerosols as CMAQ 5.1 has 23 SOAs plus
11 primarily emitted OC (POC). All of organic aerosols were assumed to have the same optical
12 properties in CRTM and RM, which is obviously an approximate assumption. Liu et al. (2016)
13 shows that SOA's optical properties could be highly varied depending on the chemical species,
14 aging time and ambient NO_x concentrations. Both CRTM and RM assume that all aerosols are
15 externally mixed, which may not best fit the situation in the real world. These uncertainties need
16 to be addressed in the future verification with observations. In this study, we only proportionally
17 adjust the aerosol mass concentrations, and did not adjust the aerosol composition, size and
18 vertical distributions which could have big impact on the AOD calculations. The data
19 assimilation for initial condition also has its limitation, and its adjustment effect could fade away
20 with time if there is persistent model bias. So, more frequent adjustment is helpful. Unfortunately
21 the MODIS AOD assimilation used in this study is applied only once per day in GSI and OI due
22 to the data availability. More satellite AOD data, such as VIIRS (Visible Infrared Imaging
23 Radiometer Suite) and GOES-R (Geostationary Operational Environmental Satellite-R Series)
24 ABT (Advanced Baseline Imager) AODs, should make this assimilation more useful. Another
25 approach is using more complex and costly four-dimensional (4-D) variational data assimilation
26 (4D-var) to correct the model's persistent biases, which integrated the data assimilation with the
27 CTM (Chai, et al., 2016). All these issue should be addressed in the future studies.

28

29 **Code Availability**

30 This study includes the forward simulations and data assimilation tools. The meteorological code
31 of WRF 3.4.1 can be downloaded from
32 http://www2.mmm.ucar.edu/wrf/users/download/get_source.html. CMAQ 5.1 can be
33 downloaded from <https://www.cmascenter.org/download.cfm>. The GSI data assimilation tool can
34 be downloaded at <http://www.dtcenter.org/com-GSI/users.v3.5/downloads/index.php>. All other
35 codes and the modified codes can be provided upon request.



Reference:

Adhikary, B., S. Kulkarni, A. Dallura, Y. Tang, T. Chai, L. R. Leung, Y. Qian, C. E. Chung, V. Ramanathan, and G. R. Carmichael. A regional scale chemical transport modeling of Asian aerosols with data assimilation of AOD observations using optimal interpolation technique. *Atmos. Environ.*, 42(37). 8600-8615, 2008.

Appel, K. W., S. J. Roselle, R. C. Gilliam, and J. E. Pleim, Sensitivity of the Community Multiscale Air Quality (CMAQ) model v4. 7 results for the eastern United States to MM5 and WRF meteorological drivers. *Geosci. Model Dev.*, 3, 169–188, 2010.

Binkowski, F. S., and S. J. Roselle, Models-3 Community Multiscale Air Quality (CMAQ) model aerosol component: 1. Model description, *J. Geophys. Res.*, 108(D6), 4183, doi:10.1029/2001JD001409, 2003.

Bocquet M., Elbern H., Eskes H., Hirtl M., Žabkar R., Carmichael G. R., Flemming J., Inness A., Pagowski M., Pérez Camacho J. L., Saide P. E.: Data assimilation in atmospheric chemistry models: current status and future prospects for coupled chemistry meteorology models. *Atmospheric chemistry and physics*;15(10):5325-58, 2015.

Chai, T. F., Carmichael, G. R., Sandu, A., Tang, Y. H., and Daescu, D. N.: Chemical data assimilation of transport and chemical evolution over the Pacific (TRACE-P) aircraft measurements, *J. Geophys. Res.*

Chai T., H.C. Kim, L. Pan, P. Lee, and D. Tong, 2017, Impact of Moderate Resolution Imaging Spectroradiometer (MODIS) aerosol optical depth (AOD) and AirNow PM2.5 assimilation on Community Multi-scale Air Quality (CMAQ) aerosol predictions over the contiguous United States, *J. Geophys. Res.*, 122, doi:10.1002/2016JD026295, 111, D02301, doi:10.1029/2006JD007763, 2006.

Chin, M., Rood, R. B., Lin, S.-J., Muller, J.-F., and Thompson, A. M.: Atmospheric sulfur cycle simulated in the global model GOCART: Model description and global properties, *J. Geophys. Res.*, 105, 24671–24687, doi:10.1029/2000JD900384, 2000.

Chin, M., Ginoux, P., Kinne, S., Torres, O., Holben, B. N., Duncan, B. N., Martin, R. V., Logan, J. A., and Higurashi, A.: Tropospheric aerosol optical thickness from the GOCART model and comparisons with satellite and Sun photometer measurements, *J. Atmos. Sci.*, 59, 461–483, 2002.

Elbern, H. and Schmidt, H.: A 4D-Var chemistry data assimilation scheme for Eulerian chemistry transport modelling, *J. Geophys. Res.*, 104, 18583–18598, 1999.

Elbern, H. and Schmidt, H.: Ozone episode analysis by four dimensional variational chemistry data assimilation, *J. Geophys. Res.*, 106, 3569–3590, 2001.



- Elbern, H., Schmidt, H., and Ebel, A.: Variational data assimilation for tropospheric chemistry modelling, *J. Geophys. Res.*, 102, 15967–15985, 1997.
- Elbern, H., Schmidt, H., Talagrand, O., and Ebel, A.: 4D-variational data assimilation with an adjoint air quality model for emission analysis, *Environ. Model. Softw.*, 15, 539–548, 2000.
- Elbern, H., Strunk, A., Schmidt, H., and Talagrand, O.: Emission rate and chemical state estimation by 4-dimensional variational inversion, *Atmos. Chem. Phys.*, 7, 3749–3769, doi:10.5194/acp-7-3749-2007, 2007.
- Han, Y., van Delst, P., Liu, Q., Weng, F., Yan, B., Treadon, R., and Derber, J.: JCSDA Community Radiative Transfer Model (CRTM) – Version 1, NOAA Tech. Rep. NESDIS 122, 33 pp., NOAA, Silver Spring, Md, 2006.
- Jiang, W., Smyth, S., Giroux, E., Roth, H., and Yin, D.: Differences between CMAQ fine mode particle and PM_{2.5} concentrations and their impact on model performance evaluation in the lower Fraser valley, *Atmos. Environ.*, 40, 4973–4985, 2006
- Lee, P., McQueen, J., Stajner, I., Huang, J., Pan, L., Tong, D., Kim, H., Tang, Y., Shafran, P., Huang, H.-C., Gorline, J., Upadhayay, S., and Artz, R.: NAQFC developmental forecast guidance for fine particulate matter (PM_{2.5}), *Weather and Forecasting*, in review. Zhao, H., Tong, D., Lee, P., Kim, H., and Lei, H, 2016: Reconstruction fire records from ground-based routine aerosol monitoring, *Atmosphere*. doi:10.1175/WAF-D-15-0163.1, 2016.
- Liu, J., P. Lin, A. Laskin, J. Laskin, S. M. Kathmann, M. Wise, R. Caylor, F. Imholt, V. Selimovic and J. E. Shilling, Optical properties and aging of light-absorbing secondary organic aerosol, *Atmos. Chem. Phys.*, 16, 12815–12827, doi:10.5194/acp-16-12815-2016, 2016.
- Liu, Z., Liu, Q., Lin, H.-C., Schwartz, C. S., Lee, Y.-H., and Wang, T.: Three-dimensional variational assimilation of MODIS aerosol optical depth: Implementation and application to a dust storm over East Asia, *J. Geophys. Res.*, 116, D22306, doi:10.1029/2011JD016159, 2011.
- Liu, Q. and Weng, F.: Advanced doubling-adding method for radiative transfer in planetary atmospheres, *J. Atmos. Sci.*, 63, 3459–3465, 2006.
- Lu, C.-H., A. da Silva, J. Wang, S. Moorthi, M. Chin, P. Colarco, Y. Tang, P. S. Bhattacharjee, S.-P. Chen, H.-Y. Chuang, H.-M. H. Juang, J. McQueen, and M. Iredell, The implementation of NEMS GFS Aerosol Component (NGAC) Version 1.0 for global dust forecasting at NOAA/NCEP, *Geosci. Model Dev.*, 9, 1905-1919, doi:10.5194/gmd-9-1905-2016, 2016.
- Malm, W. C., J. F. Sisler, D. Huffman, R. A. Eldred, and T. A. Cahill, Spatial and seasonal trends in particle concentration and optical extinction in the United States, *J. Geophys. Res.*, 99, 1347–1370, 1994.



Pagowski, M., Z. Liu, G. A. Grell, M. Hu, H.-C. Lin, C. S. Schwartz: Implementation of aerosol assimilation in Gridpoint Statistical Interpolation (v. 3.2) and WRF-Chem (v. 3.4.1), *Geosci. Model Dev.*, 7, 1621–1627, doi:10.5194/gmd-7-1621-2014., 2014.

Pan, L., D.Q. Tong, P. Lee, H. Kim and T. Chai, Assessment of NO_x and O₃ forecasting performances in the U.S. National Air Quality Forecasting Capability before and after the 2012 major emissions updates, *Atmospheric Environment*, 95, 610-619. doi:10.1016/j.atmosenv.2014.06.020, 2014.

Parrish D. F. and Derber J. C.: The National Meteorological Center spectral statistical interpolation analysis system, *Mon. Weather Rev.*, 120, 1747–1763, 1992.

Purser, R. J., Wu, W.-S., Parrish, A. F., and Roberts, N. M.: Numerical aspects of the application of recursive filters to variational statistical analysis. Part I: Spatially homogeneous Gaussian covariances, *Mon. Weather Rev.*, 131, 1524–1535, 2003a.

Purser, R. J., Wu, W.-S., Parrish, A. F., and Roberts, N. M.: Numerical aspects of the application of recursive filters to variational statistical analysis. Part II: Spatially inhomogeneous and anisotropic general covariances, *Mon. Weather Rev.*, 131, 1536–1549, 2003b.

Roy, B., R. Mathur, A. B. Gilliland, and S. C. Howard, A comparison of CMAQ-based aerosol properties with IMPROVE, MODIS, and AERONET data, *J. Geophys. Res.*, 112, D14301, doi:10.1029/2006JD008085, 2007.

Sonntag, D. B., R. W. Baldauf, C. A. Yanca and C. R. Fulper, Particulate matter speciation profiles for light-duty gasoline vehicles in the United States, *Journal of the Air & Waste Management Association*, 64:5, 529-545, DOI:10.1080/10962247.2013.870096, 2014.

Tang, Y., T. Chai, L. Pan, P. Lee, Daniel Tong, H. Kim, and W. Chen, Using Optimal Interpolation to Assimilate Surface Measurements and Satellite AOD for Ozone and PM_{2.5}: A Case Study for July 2011. *Journal of the Air & Waste Management Association*, DOI:10.1080/10962247.2015.1062439, 2015.

Tang, Y., P. Lee, M. Tsidulko, H.-C. Huang, J. T. McQueen, G. J. DiMego, L. K. Emmons, R. B. Pierce, A. M. Thompson, H.-M. Lin, D. Kang, D. Tong, S.-C. Yu, R. Mathur, J. E. Pleim, T. L. Otte, G. Pouliot, J. O. Young, K. L. Schere, P. M. Davidson and I. Stajner, The Impact of chemical lateral boundary conditions on CMAQ predictions of tropospheric ozone over the Continental United States, *Environmental Fluid Mechanics*, doi:10.1007/s10652-008-9092-5, 2008.

Whitby, E. R., and P. H. McMurry, Modal aerosol dynamics modeling. *Aerosol Science and Technology* 27: 673-688, 1997.



Wu, W.-S., Purser, R. J., and Parrish, D. F.: Three-dimensional variational analysis with spatially inhomogeneous covariances, *Mon. Weather Rev.*, 130, 2905–2916, 2002.



Table 1. CMAQ 5.1 aerosol species and their Mapping to GOCART aerosol optical properties in CRTM. (CMAQ species with solid underline are Aitken-mode aerosols, and those with dash underline are coarse-mode aerosols, and the rest are the accumulation-mode aerosols)

Aerosol Species in CMAQ 5.1	GOCART aerosols in CRTM
<u>ASO4I</u> <u>ANO3I</u> <u>ANH4I</u> <u>ACLI</u> <u>ASO4J</u> <u>ANO3J</u> <u>ANH4J</u> <u>ASO4K</u> <u>ANO3K</u> <u>ANH4K</u>	Sulfate Aerosol
<u>AECI</u> <u>AECJ</u>	Black Carbon Aerosol
<u>APOCI</u> <u>APNCOMI</u> <u>APOCJ</u> <u>AOTHRJ</u> <u>AXYL1J</u> <u>AXYL2J</u> <u>AXYL3J</u> <u>ATOL1J</u> <u>ATOL2J</u> <u>ATOL3J</u> <u>ABNZ1J</u> <u>ABNZ2J</u> <u>ABNZ3J</u> <u>AISO1J</u> <u>AISO2J</u> <u>AISO3J</u> <u>ATRP1J</u> <u>ATRP2J</u> <u>ASQTJ</u> <u>AALK1J</u> <u>AALK2J</u> <u>AORGJ</u> <u>AOLGBJ</u> <u>AOLGAJ</u> <u>APAH1J</u> <u>APAH2J</u> <u>APAH3J</u> <u>APNCOMJ</u>	Organic Carbon Aerosol
<u>AFEJ</u> <u>AALJ</u> <u>ASIJ</u> <u>ACAJ</u> <u>AMGJ</u> <u>AKJ</u> <u>AMNJ</u> <u>ACORS</u> <u>ASOIL</u>	Dust Aerosol
<u>ANAJ</u> <u>ACLJ</u> <u>ACLK</u> <u>ASEACAT</u>	Sea Salt Aerosol



Table 2. Regional statistic of the three simulations (CMAQ_BASE, OI and GSI) for surface PM_{2.5} in July, 2011

Regions	Simulations	Mean Bias (µg/m ³)	Root Mean Square Error (µg/m ³)	Correlation Coefficient, R	Index of Agreement
CONUS	BASE	-2.25	10.57	0.3	0.54
	OI	0.77	11.07	0.38	0.59
	GSI	-0.73	9.42	0.44	0.64
Northeastern USA	BASE	-3.36	11.02	0.27	0.54
	OI	0.78	11.17	0.42	0.64
	GSI	-1.18	9.70	0.44	0.66
Pacific Coast	BASE	-2.24	8.74	0.23	0.40
	OI	0.71	9.13	0.40	0.60
	GSI	-0.80	7.86	0.44	0.61
Southeastern USA	BASE	-1.86	11.05	0.23	0.50
	OI	0.12	9.88	0.41	0.63
	GSI	-0.58	9.30	0.41	0.63
Rocky Mountain States	BASE	-3.22	12.14	0.09	0.24
	OI	1.59	13.28	0.13	0.30
	GSI	-1.63	11.75	0.16	0.28
North Central	BASE	-1.55	12.29	0.22	0.49
	OI	0.96	13.83	0.28	0.51
	GSI	-0.26	11.12	0.35	0.59
South Central	BASE	-1.1	9.49	0.09	0.4
	OI	0.38	8.07	0.27	0.52
	GSI	-0.1	7.58	0.27	0.54

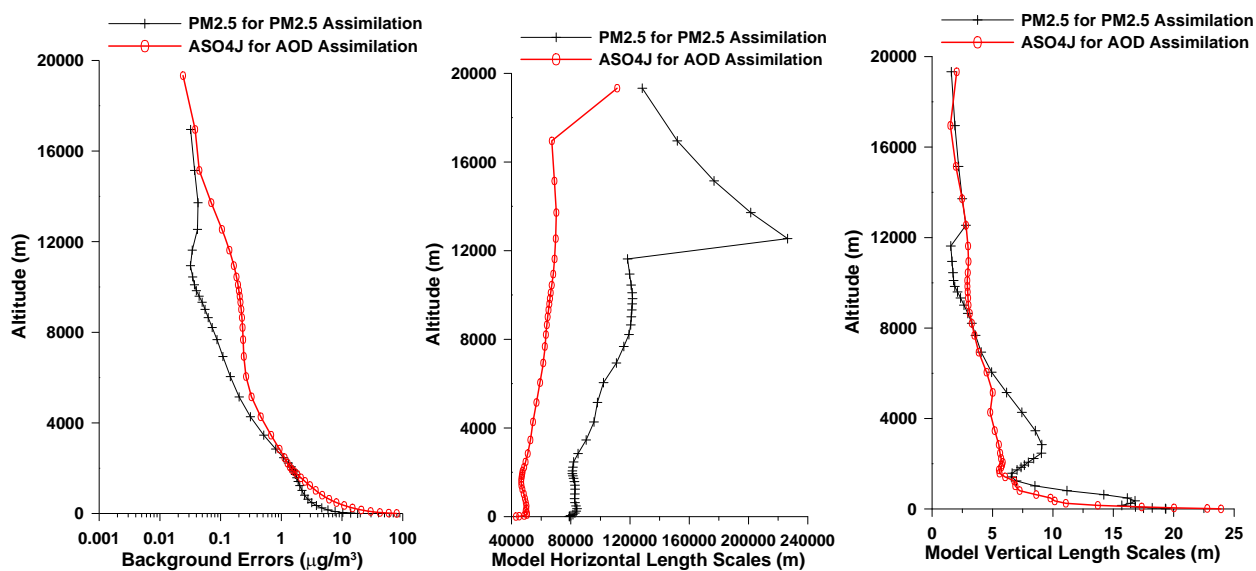


Figure 1. GSI's background errors and length scales used in this study (ASO4J is the CMAQ's accumulation-mode sulfate aerosol)

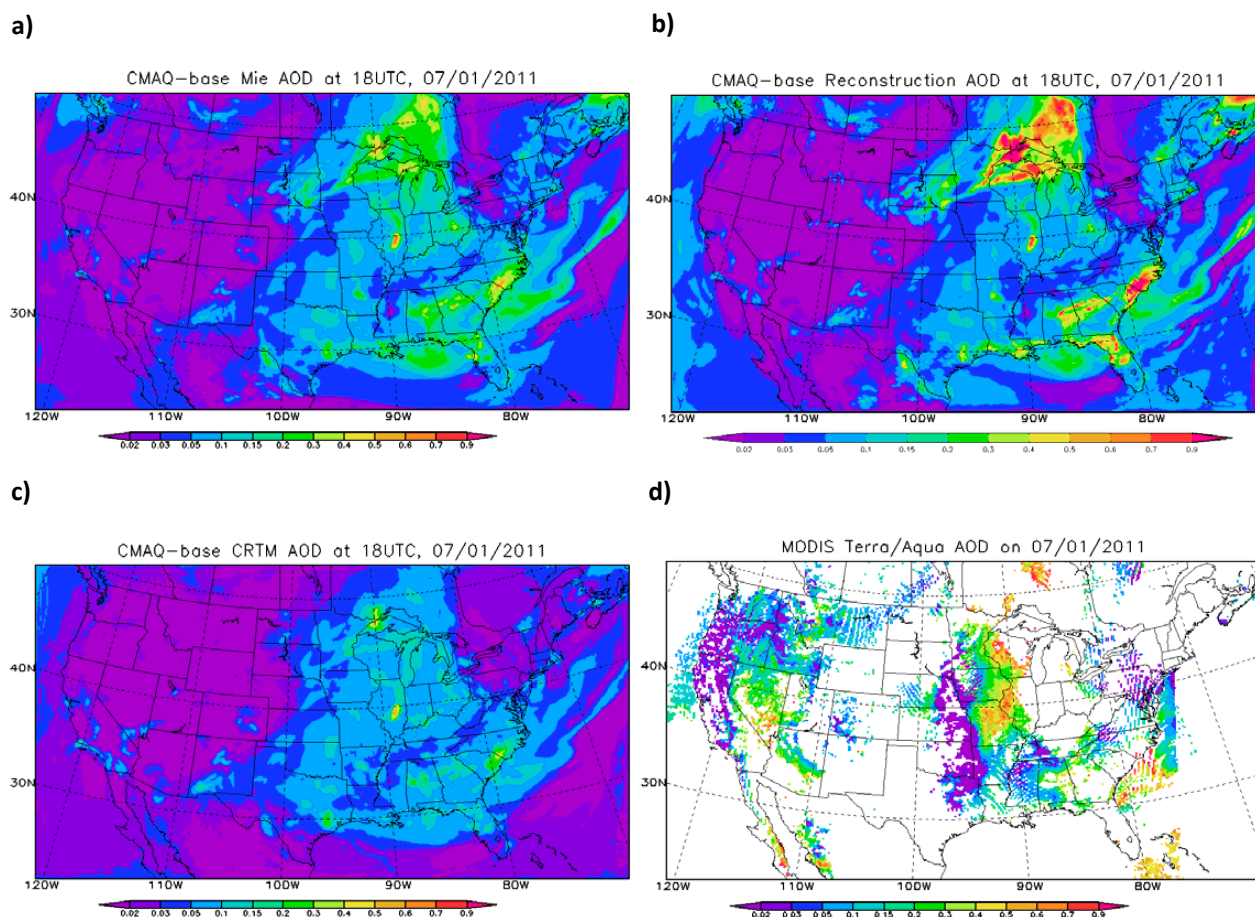


Figure 2, AOD calculations using Mie-method (a), reconstruction method (b), and CRTM from the CMAQ's base case (before assimilations) compared to MODIS AOD on 07/01/2011.

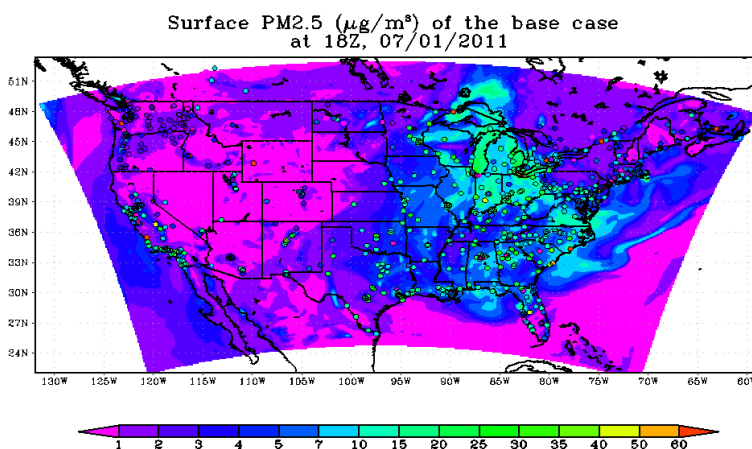


Figure 3. Predicted surface PM_{2.5} from CMAQ base run compared to surface measurement (close circle) at 18 UTC, 07/01/2011.

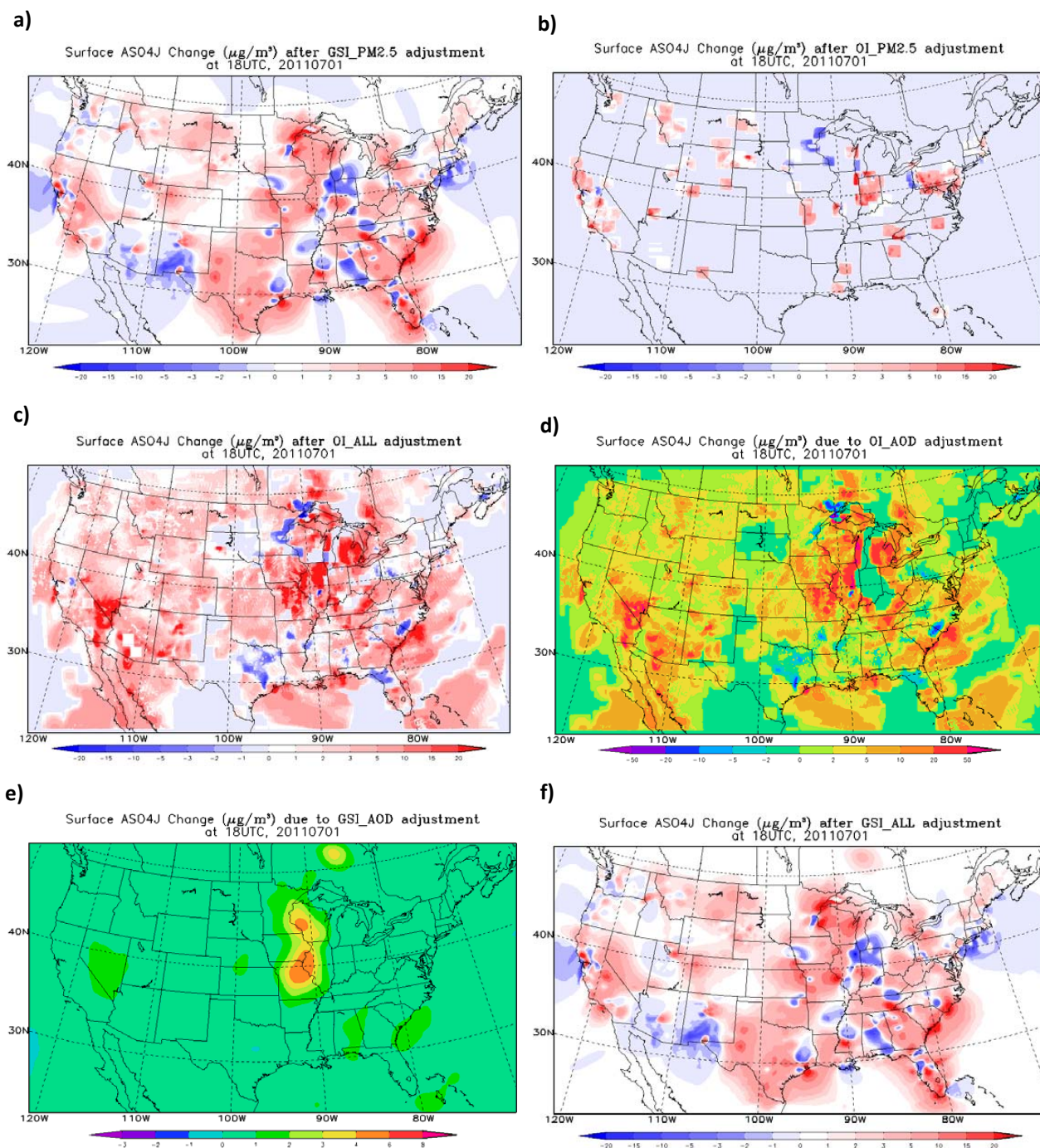


Figure 4. surface accumulation-mode sulfate (ASO4J) changes after GSI (left) and OI (right) assimilations with surface PM_{2.5} and AOD.



Model Predicted PBL Height (m) at 18UTC, 07/01/2011

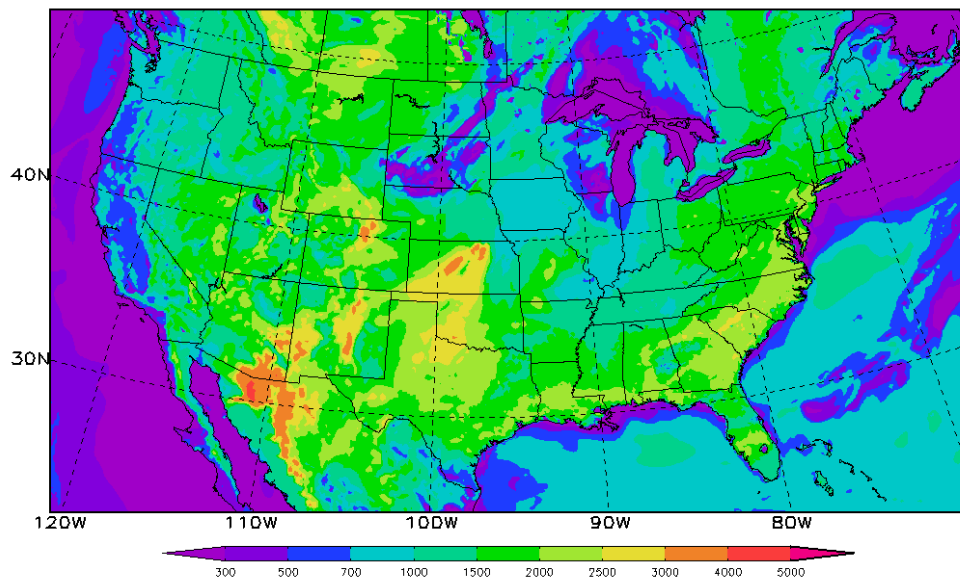


Figure 5. Model-Predicted PBL height (m) at 18UTC, 07/01/2011

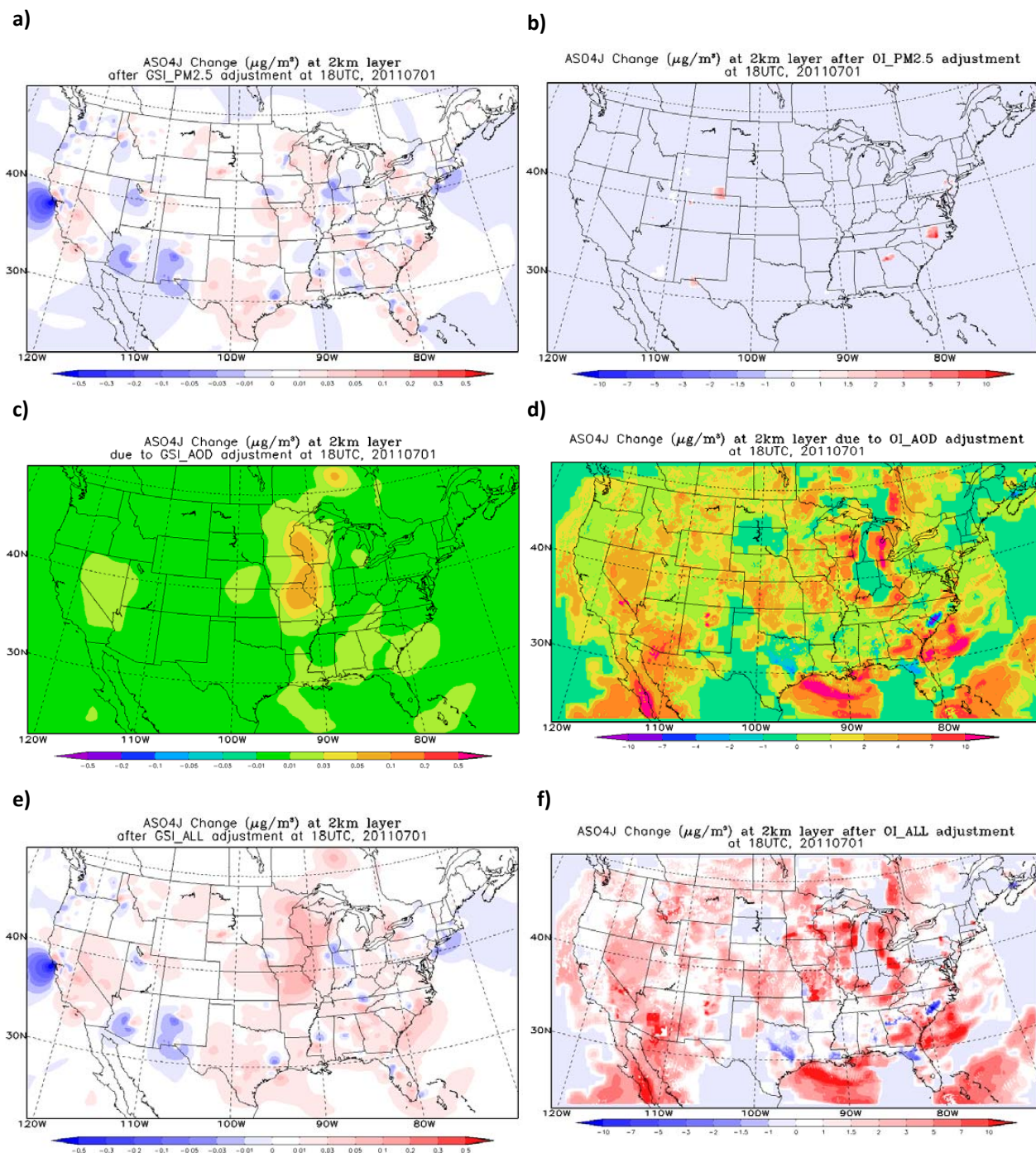


Figure 6, same as the figure 4 but for the model's 2km layer.

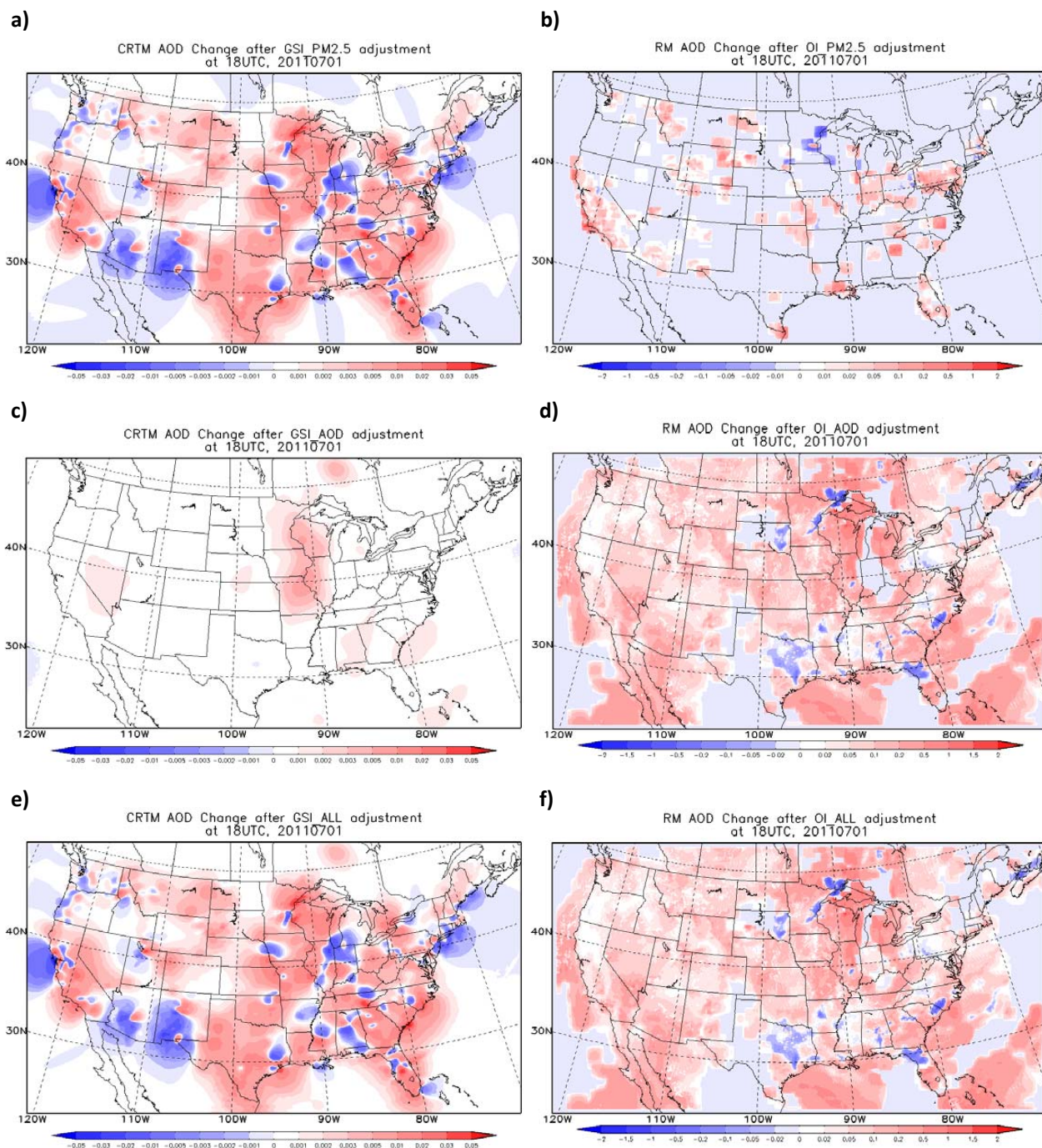
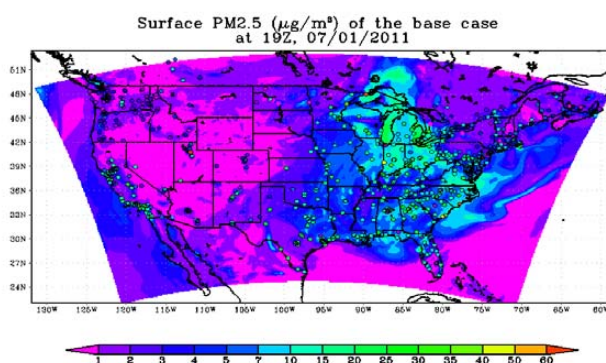


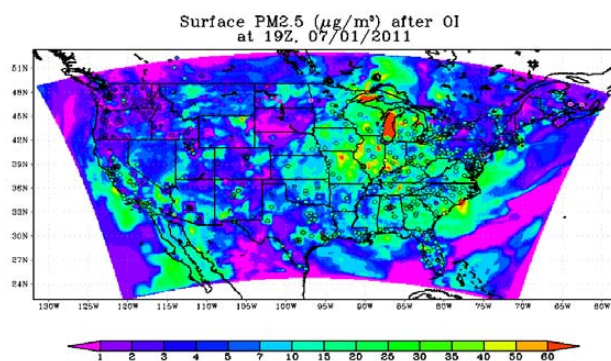
Figure 7, same as the Figure 4 but for AOD change. Left plots show the CRTM AOD change due to GSI adjustments and right plots are RM AOD change for OI.



a)



b)



c)

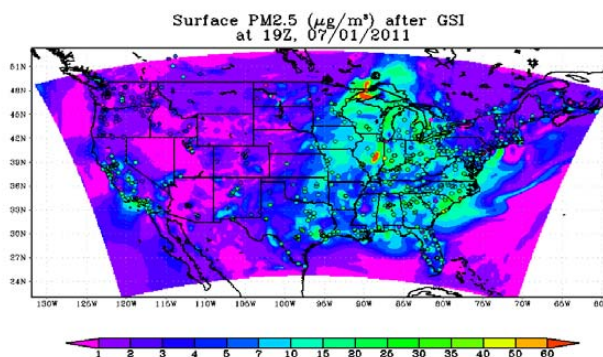


Figure 8, Predicted surface PM_{2.5} from the base case (a), OI (b) and GSI (c) runs compared to surface observation at 19UTC, 07/01/2011.

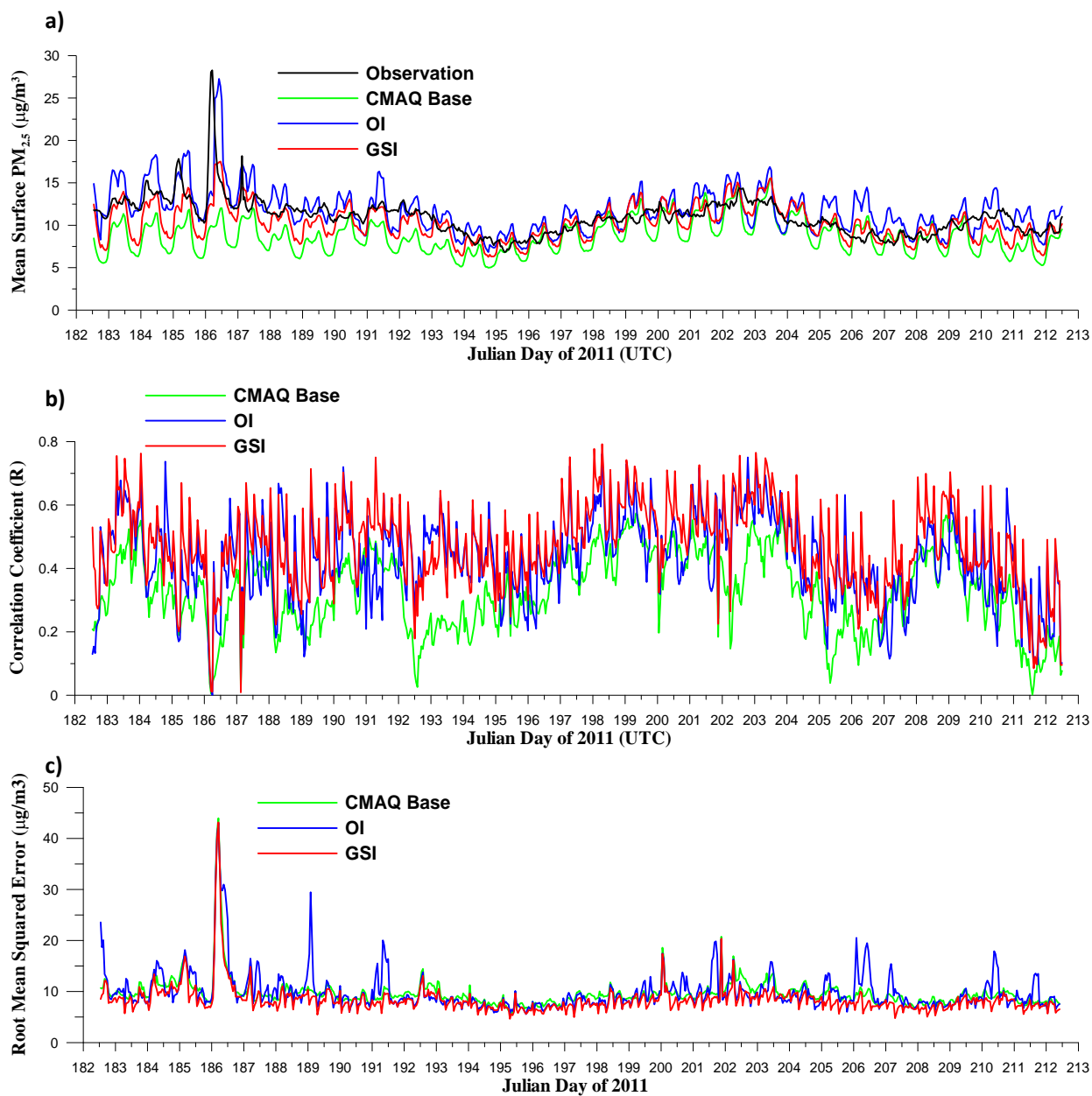


Figure 9, Time-series comparisons of CMAQ surface $PM_{2.5}$ (base, OI, and GSI) versus the observation over the CONUS domain for their mean value (a), correlation coefficient (b) and root mean squared error (RMSE) (c)